Anisotropies in the optical ac and dc conductivities in lightly doped $La_{2-x}Sr_xCuO_4$: the role of deep and shallow acceptor states

2011 J. Phys.: Condens. Matter 23 215602

(http://iopscience.iop.org/0953-8984/23/21/215602)

J. Phys.: Condens. Matter **23** (2011) 215602 (9pp) doi:10.1088/0953-8984/23/21/215602

Anisotropies in the optical ac and dc conductivities in lightly doped $La_{2-x}Sr_xCuO_4$: the role of deep and shallow acceptor states

M B Silva Neto[1], G Blumberg[2], A Gozar[3], Seiki Komiya[4] and Yoichi Ando[5]

[1] Instituto de Física, Universidade Federal do Rio de Janeiro, Caixa Postal 68528, Rio de Janeiro, Brazil
[2] Department of Physics and Astronomy, Rutgers University, Piscataway, NJ 08854-8019, USA
[3] Brookhaven National Laboratory, Upton, NY 11973-5000, USA
[4] Central Research Institute of Electric Power Industry, Yokosuka, Kanagawa 240-0196, Japan
[5] Institute of Scientific and Industrial Research, Osaka University, Ibaraki, Osaka 567-0047, Japan

Received 4 March 2011, in final form 7 April 2011
Published 11 May 2011
Online at stacks.iop.org/JPhysCM/23/215602

Abstract

We investigate the origin of the optical ac and dc conductivity anisotropies observed in the low temperature orthorhombic phase of lightly doped, untwinned $La_{2-x}Sr_xNiO_4$ single crystals. We show that these anisotropies can be naturally ascribed to the emergence of two odd parity, rotational-symmetry-broken, localized impurity acceptor states, one deeper and one shallower, resulting from the trapping of doped holes by the Coulomb potential provided by the Sr ions. These two lowest-energy, p-wave-like states are split by orthorhombicity and are partially filled with holes. This leaves a unique imprint in the optical ac conductivity, which shows two distinct far-infrared continuum absorption energies corresponding to the photoionization of the deep and shallow acceptor states. Furthermore, we argue that the existence of two independent and orthogonal channels for hopping conductivity, directly associated with the two orthorhombic directions, also quantitatively explains the observed low temperature anisotropies in the dc conductivity.

(Some figures in this article are in colour only in the electronic version)

1. Introduction

Understanding the evolution from a Mott insulating behavior until the realization of high temperature superconductivity in lamellar copper oxides is one of the most challenging problems in condensed matter physics. It is widely agreed that t–J-like models already capture the essential features of underdoped cuprates [1], such as a small Fermi surface (FS) composed of four pockets located at special positions in the magnetic Brillouin zone [2]. However, while the rather low frequency of quantum Hall oscillations observed in $YBa_2Cu_3O_{6.5}$ [3], as well as the de Haas–van Alphen effect [4], support the small FS scenario, the validity of such a strong coupling, single-band description has recently been put under scrutiny, after a new analysis of the optical conductivity spectra in $La_{2-x}Sr_xCuO_4$ [5]. Furthermore, the interplay between spin, charge and orbital degrees of freedom, together with disorder, makes any theoretical description of such systems a very difficult task. Such a large degree of complexity can be significantly reduced by the thorough analysis of magnetic, optical and transport experiments, such as the ones performed in untwinned $La_{2-x}Sr_xCuO_4$ single crystals, the simplest representative of this class of compounds [6]. Understanding these experiments might also help us clarify the role of interactions in cuprates.

Infrared (IR) spectroscopy is a very useful tool to investigate charge dynamics in metals and semiconductors. The analysis of the far-IR (FIR) ac conductivity spectrum of $La_{2-x}Sr_xCuO_4$, for $x = 0.03$ and 0.04, by Dumm *et al* [7], revealed that: (i) at high temperature, $T > 80$ K, a Drude-like response is observed, suggesting that the electronic conductivity is band-like even for such low doping, which is consistent with the mobility analysis of the dc conductivity [8] and (ii) at lower temperature, instead, the suppression of the Drude-like behavior in the FIR, with the observation of a peak centered at finite frequency ω, points toward the localization of charge carriers [9], much like as it happens in doped semiconductors, strongly disordered metals and other cuprate superconductors [10]. The position of such a peak can, in turn, be associated with the typical energy scale for localization, the binding energy of the holes. Most remarkable, however, is the observation of two distinct absorption energies for two specific polarizations of the incident light, namely along the two orthorhombic axis, hereby referred to as A and B channels (according to this notation, A means that the incident light is polarized along the A orthorhombic direction and is absorbed, no emission) [7].

The dc conductivity in lightly doped $La_{2-x}Sr_xCuO_4$ can also be divided into two main regimes: metallic (band-like) and insulating (hopping) [8, 11]. At higher to moderate temperatures, when all hole-like carriers have been activated to the valence band, a simple Drude picture for the hole conductivity:

$$\sigma = \frac{ne^2\tau}{m^*}, \tag{1}$$

is able to explain (surprisingly) quite well the rather weakly anisotropic dc conductivity data. At lower temperature, however, when the holes become localized around the Sr dopants, hopping conductivity between impurity sites becomes the dominant mechanism for the transport. Quite unexpectedly, such hopping transport is also found to be clearly anisotropic and exhibits two different temperature scales for the onset of localization [11], sometimes called freezing-out temperatures [12], depending on the direction of the applied electric field.

In this work, we investigate the origin of the anisotropies in the optical ac and dc conductivity responses described above, observed in the low temperature orthorhombic phase of lightly doped, untwinned $La_{2-x}Sr_xCuO_4$ single crystals. As we shall clarify below, although stripe formation has been successfully used before to explain the mid-IR (MIR) optical spectra of $La_{2-x}Sr_xNiO_4$ and $La_{2-x}Sr_xCuO_4$ for $x > 0.055$ [13], for the case of insulating $La_{2-x}Sr_xCuO_4$, $x < 0.055$, where holes are localized by the Coulomb potential provided by the randomly distributed Sr impurities, the two energy scales found in the FIR ac response are associated, instead, with the two lowest-energy, parity-odd, rotational-symmetry-broken p-wave impurity states. These provide also two independent and orthogonal channels for hopping conductivity which naturally explain the low temperature dc conductivity anisotropies [11]. The relationship between a rotational non-invariant impurity state and anisotropic dc response has already been acknowledged in [14], where the deformation of a single, parity-even, hydrogenic 1s orbital, due to the formation of antiferromagnetic spin spirals, was considered. Here we show that the selection rules for IR absorption are consistent, actually, with two parity-odd p-wave orbitals [7].

2. Electronic structure

According to recent exact diagonalization studies by Chen, Rice and Zhang, for the t–t'–J model on a square lattice [15], the ground state for a hole bound to an Na charged impurity at the center of a four-Cu plaquette in $Ca_{2-x}Na_xCuO_2Cl_2$ is doubly degenerate and parity-odd. These results are in agreement with earlier numerical studies by Rabe and Bhatt [16], as well as Gooding [17], for the case of an Sr impurity in $La_{2-x}Sr_xCuO_4$, which is the case we shall consider in the present work. Although the Sr ion is actually located above a four-Cu plaquette, the rather large extent of the doped-hole-Sr-ion bound state allows us to neglect, in what follows, the small displacement of the Sr impurity from the plane.

The presence of the Sr impurity in $La_{2-x}Sr_xCuO_4$ breaks the translational symmetry of the square lattice and the different possible localized states can be classified according to the irreducible representations of the C_{4v} point group, labeled by the eigenvalues of the reflection operators P_x and P_y, (P_x, P_y) [15]. Because of the existence of the antiferromagnetic background, the ground state is found to be doubly degenerate and belongs then to a two-dimensional, E, representation which corresponds to the degenerate $(+, -)$ and $(-, +)$ states [15, 16]. There is a third, fully symmetric low-lying excited s-wave state which belongs to A_1, labeled by $(+, +)$, and a fourth, higher energy, d-wave state belonging to B_2, labeled by $(-, -)$ [15]. For the continuum part of the spectrum, the single delocalized hole state of the t–t'–J model is labeled by its momentum $\mathbf{k}$ and corresponds to the maxima of the weakly elliptical hole pockets centered at $(\pm\pi/2, \pm\pi/2)_g$ (in units $a = 1$), see figure 1.

In what follows, however, it will be more convenient to: (i) first extend the square lattice to a tetragonal structure; and afterwards (ii) to consider explicitly the symmetry reduction in $La_{2-x}Sr_xCuO_4$ from the high temperature tetragonal (HTT) phase, with crystal structure $I4/mmm$ and point group D_{4h}, down to the low temperature orthorhombic (LTO) phase, with $Bmab$ crystal structure and associated D_{2h} point group. Here a and b are the two planar orthorhombic axis, shown in figure 1, with $b > a$. In this case, the double degeneracy of the ground state is lifted by the orthorhombicity, and the character of the parity-odd ground state is reduced following

$$E_u \rightarrow B_{2u} + B_{3u}. \tag{2}$$

Analogously, the higher energy states are also reduced according to standard group theoretical rules:

$$A_{1g} \rightarrow A_g^s \qquad B_{2g} \rightarrow A_g^d. \tag{3}$$

Finally, the single delocalized hole state, labeled by $(\pm\pi/2, \pm\pi/2)_g$, also has its symmetry modified from

$$B_{2g} \rightarrow A_g. \tag{4}$$

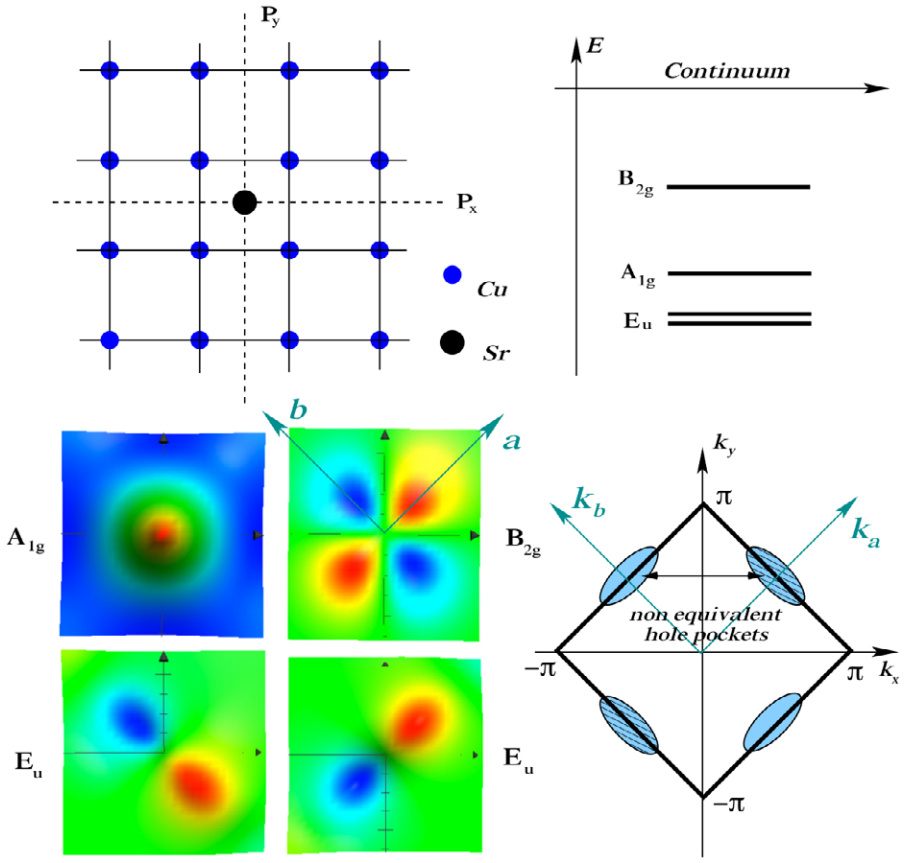

Figure 1. Top left: Sr ion at the center of a four-Cu plaquette and the reflection axis P_x, P_y. Top right: localized energy levels and their irreducible representations of the D_{4h} point group. The ground state E_u is doubly degenerate and parity-odd (note that we are using the hole picture here, so the energy axis is reversed). Bottom left: A_{1g}, B_{2g} and E_u wavefunctions. Bottom right: the delocalized hole has dispersion with maxima at $(\pm\pi/2, \pm\pi/2)$ and belongs to B_{2g}.

2.1. Structure of acceptor states

Following Kohn and Luttinger (KL) [18], the wavefunctions corresponding to the $i = B_{3u}, B_{2u}, A_g^s, A_g^d$ states can be generally written as

$$\Psi_i(\mathbf{r}) = \sum_\mu \alpha_\mu^i F^i(\mathbf{r})\phi(\mathbf{k}_\mu, \mathbf{r}), \tag{5}$$

where

$$\phi(\mathbf{k}_\mu, \mathbf{r}) = e^{i\mathbf{k}_\mu\cdot\mathbf{r}} u_{\mathbf{k}_\mu}(\mathbf{r}) \tag{6}$$

and $u_{\mathbf{k}_\mu}(\mathbf{r})$ is a periodic Bloch wavefunction with minima at $\mathbf{k}_\mu = \mathbf{k}_{a,b}^{\pm}$. The index μ runs over the

$$\mathbf{k}_a^+ = (\pi/2, \pi/2), \qquad \mathbf{k}_b^+ = (-\pi/2, \pi/2),$$

$$\mathbf{k}_a^- = (-\pi/2, -\pi/2), \qquad \mathbf{k}_b^- = (\pi/2, -\pi/2)$$

pockets (we use here the tetragonal notation for clarity) and the envelope functions calculated within the effective mass approximation at each pocket are

$$F^i(\mathbf{r}) = \frac{1}{\sqrt{\pi\xi_i^2}} e^{-r/\xi_i}. \tag{7}$$

Here $r = \sqrt{x^2 + y^2}$ and ξ_i controls the exponential decay of the wavefunction for the ith impurity level. Finally, the coefficients

$$\alpha_\mu^{B_{3u}} = \frac{1}{\sqrt{2}}(1, 0, -1, 0) \qquad \alpha_\mu^{B_{2u}} = \frac{1}{\sqrt{2}}(0, 1, 0, -1)$$

$$\alpha_\mu^{A_g^s} = \tfrac{1}{2}(1, 1, 1, 1) \qquad \alpha_\mu^{A_g^d} = \tfrac{1}{2}(1, -1, 1, -1)$$

provide the correct parity properties to the four localized states and are determined by the relevant symmetries of the orthorhombic *Bmab* point group [18].

The two lowest-energy B_{3u} and B_{2u} localized states correspond, respectively, to the parity-odd p-wave-like orbitals along the two orthorhombic directions, a and b, see figure 1, given explicitly by

$$\Psi_{B_{3u}}(x, y) = \frac{1}{\sqrt{2\pi\xi_{B_{3u}}}} \sin\left[\frac{\pi(x+y)}{2}\right] e^{-r/\xi_{B_{3u}}} u_{(\frac{\pi}{2},\frac{\pi}{2})}(\mathbf{r}),$$

$$\Psi_{B_{2u}}(x, y) = \frac{1}{\sqrt{2\pi\xi_{B_{2u}}}} \sin\left[\frac{\pi(x-y)}{2}\right] e^{-r/\xi_{B_{2u}}} u_{(\frac{\pi}{2},\frac{\pi}{2})}(\mathbf{r}),$$

where $\xi_{B_{3u},B_{2u}}$ are the localization lengths for the two p-wave-like states, B_{3u} and B_{2u}, oriented along the a and b directions, respectively.

At this point one comment is in order. The unusual aspect of the above results, namely having two antisymmetric p-wave states with lower energy than the fully symmetric s-wave one, is a direct consequence of the existence of a nontrivial antiferromagnetic background for the doped holes. In fact, upon doping, the holes will prefer to localize in states that correspond to sublattices with a definite spin projection, to avoid the energy cost of antiferromagnetic superexchange, J, for moving between different sublattices. This is exactly the case of the two B_{2u} and B_{3u} states described above, which, due to the auspicious geometry of the Sr impurity at the center of a four-Cu plaquette, can be straightforwardly associated with the two different spin-up and spin-down sublattices. This also reminds us that physics of acceptor states in strongly correlated Mott insulators, like $La_{2-x}Sr_xCuO_4$, is much more involved than for the case of simple semiconductors.

The wavefunctions for the other two higher energy orthorhombic states can also be calculated analogously and we find

$$\begin{aligned}\Psi_{A_g^s}(x,y) &= \frac{1}{\sqrt{2\pi\xi_{A_g^s}}}\left(\cos\left[\frac{\pi(x+y)}{2}\right]\right.\\ &\left.+\ \cos\left[\frac{\pi(x-y)}{2}\right]\right)e^{-r/\xi_{A_g^s}}u_{(\frac{\pi}{2},\frac{\pi}{2})}(\mathbf{r}),\\ \Psi_{A_g^d}(x,y) &= \frac{1}{\sqrt{2\pi\xi_{A_g^d}}}\left(\cos\left[\frac{\pi(x+y)}{2}\right]\right.\\ &\left.-\ \cos\left[\frac{\pi(x-y)}{2}\right]\right)e^{-r/\xi_{A_g^d}}u_{(\frac{\pi}{2},\frac{\pi}{2})}(\mathbf{r}),\end{aligned} \tag{8}$$

where $\xi_{A_g^s},\xi_{A_g^s}$ are the localization lengths for the two parity-even states, A_g^s and A_g^d. In figure 1 we show all four localized state wavefunctions. It should also be stressed here that the KL Ψ_i wavefunctions calculated above, do not include the information that the delocalized holes are incoherent over a large part of the Fermi [2]. This will be addressed elsewhere [19], but for now it suffices to acknowledge the anisotropic p-orbital shape of the lowest-energy impurity states (see figure 1).

For perfectly tetragonal systems, such as the $Ca_{2-x}Na_xCuO_2Cl_2$ system discussed previously, we have that $\xi_{B_{3u}} = \xi_{B_{2u}} = \xi_0$, and a complex linear combination of the wavefunctions corresponding to the degenerate B_{2u} and B_{3u} levels can, in principle, be constructed: $\Psi^{\pm}_{E_u}(x,y) = \Psi_{B_{2u}}(x,y) \pm i\Psi_{B_{3u}}(x,y)$. To such a wavefunction one can associate an orbital angular momentum and they would correspond to the chiral wavefunctions proposed long ago by Gooding, describing states circulating clockwise and counterclockwise around the dopant [17]. For the $La_{2-x}Sr_xCuO_4$ system, however, the degeneracy is lifted by the orthorhombic distortion and AF order, thus quenching completely this orbital motion. Observe, furthermore, that the envelope wavefunctions calculated here are not truly of the p-wave type since there are no x, y, or r dependences in the exponential pre-factor.

Finally, the orthorhombic splitting $E_u \rightarrow B_{3u} + B_{2u}$ is determined by the competition between the Coulomb potential from the Sr ion, which favors a B_{3u} ground state ($b > a$), and the next-to-nearest-neighbor hopping $t'_a > t'_b$ [20], which favors a B_{2u} ground state. In what follows we shall argue that: (i) for $x = 0.01$, when the Sr ion is poorly screened, the B_{3u} state becomes the ground state and (ii) for $x = 0.03$, instead, the B_{2u} state becomes the ground state (most likely due to better screening), causing a switch of the dc conductivity anisotropies (a related switch is also observed in the Raman intensity anisotropies [21]).

3. Optical ac conductivity

3.1. Localization of carriers

As mentioned in section 1, the observation of a peak at finite frequency in the optical conductivity spectrum of $La_{2-x}Sr_xCuO_4$, followed by a suppression of the Drude behavior at low frequencies, is consistent with the strong localization of doped carriers. On general grounds, the $T = 0$ optical conductivity can be calculated as proposed by Vollhardt and Wölfle [9] and is given by

$$\sigma(\omega) = e^2\frac{n}{m^*}\frac{i}{\omega + M(0,\omega)} = \sigma'(\omega) + i\sigma''(\omega), \tag{9}$$

where e is the electric charge, n is the carrier density, m^* is the effective mass and the memory function is given as $M(0,\omega) = i/\tau$ for a metal with relaxation time τ and

$$M(0,\omega) = \frac{i}{\tau} - \frac{\omega_0^2}{\omega}, \tag{10}$$

for a disordered insulator. The insulating character of the above expression arises from the infrared divergence of the memory function as $\omega \rightarrow 0$, which is in turn characterized by a single oscillator with frequency given by ω_0. In our case, such an oscillator frequency can be directly associated with the typical binding energy of the acceptor states and determines their localization length [9]. For the case of two localized states, one deep and one shallow, we obtain, for the real part of the conductivity:

$$\sigma'(\omega) = \frac{e^2n}{m^*}\frac{1/\tau}{(\omega - \omega_0^2/\omega)^2 + (1/\tau)^2}, \tag{11}$$

a behavior similar to the one depicted in figure 2. At finite temperature, lattice vibrations (phonons) promote the tunneling of carriers between impurity states, producing a finite value for $\sigma(\omega)$ even at $\omega = 0$, consistent with the optical experiments by Dumm *et al* [7] and also consistent with the low temperature hopping dc conductivity [11].

3.2. IR selection rules

The finite frequency peaks observed in the optical ac spectrum of $La_{2-x}Sr_xCuO_4$ for $x = 0.03, 0.04$ [7] are related to the absorption, by the continuum, of the photoionized hole states, made possible by the electric-dipole coupling. Within the framework of the D_{2h} group, a dipole along the a/b axis belongs to the B_{3u}/B_{2u} irreducible representations, respectively. At the top of the valence band maximum, located

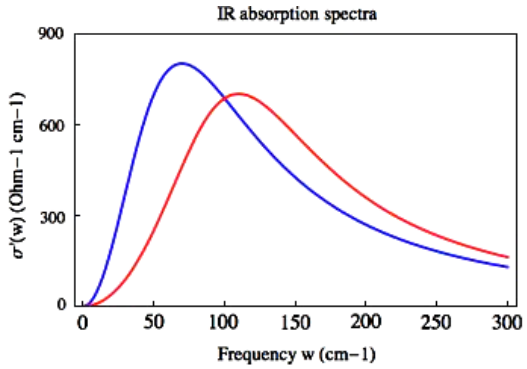

Figure 2. Typical behavior for the real part of the optical conductivity, $\sigma'(\omega)$, from equation (11), in lightly doped $La_{2-x}Sr_xCuO_4$. The two continuum absorption energies correspond to the photoionization of the two possible types of localized states: the deep/red and shallow/blue acceptor states.

at the $\mathbf{k}_0 = (\pm\pi/2, \pm\pi/2)$ points in the Brillouin zone, a delocalized hole is accessible at the A_g channel of the orthorhombic D_{2h} group (or, equivalently, the B_{2g} channel of the tetragonal point group D_{4h}), as recently demonstrated by Tassini *et al* in [22].

According to the above reasoning, the only electric-dipole transitions, allowed by group symmetry, between the bound and delocalized hole states are (see figure 3):

(i) absorption of a B_{3u} hole at ε_A for $E \parallel a$, since

$$B_{3u} \times B_{3u} = A_g, \tag{12}$$

(ii) absorption of a B_{2u} hole at ε_B for $E \parallel b$, since

$$B_{2u} \times B_{2u} = A_g. \tag{13}$$

The above selection rules are very important because: (i) they determine precisely the types of absorption processes allowed, constraining the photoionization of each state to each of the orthorhombic directions, and (ii) they determine unambiguously the odd parity of the impurity ground state, see figure 3.

3.3. Orthorhombic splitting

The energy difference between the ac peaks at $\varepsilon_0 - \varepsilon_A$, for the A channel, and at $\varepsilon_0 - \varepsilon_B$, for the B channel, is a direct measure of the orthorhombic level splitting. For $x = 0.03$ and 0.04 such a splitting is ∼30 K [7], The localization lengths, $\xi_{A,B}$, relate to the binding energies as $(\varepsilon_0 - \varepsilon_{A,B}) \sim \xi_{A,B}^{-2}$, and typically $\xi_B \approx 2 - 2.5$ in units of a. For $x = 0.03$ and 0.04 the B_{3u} state is shallower than the B_{2u} state, see figure 4, and we find $\xi_A > \xi_B$. For $x = 0.01$, in turn, we shall argue that this situation is reversed, causing the dc anisotropy switch [21].

3.4. Disorder bandwidth

Each Sr ion doped into $La_{2-x}Sr_xCuO_4$ acts as an acceptor and introduces precisely one hole into the system. Nevertheless, a sizable bandwidth of disorder W can allow for unoccupied

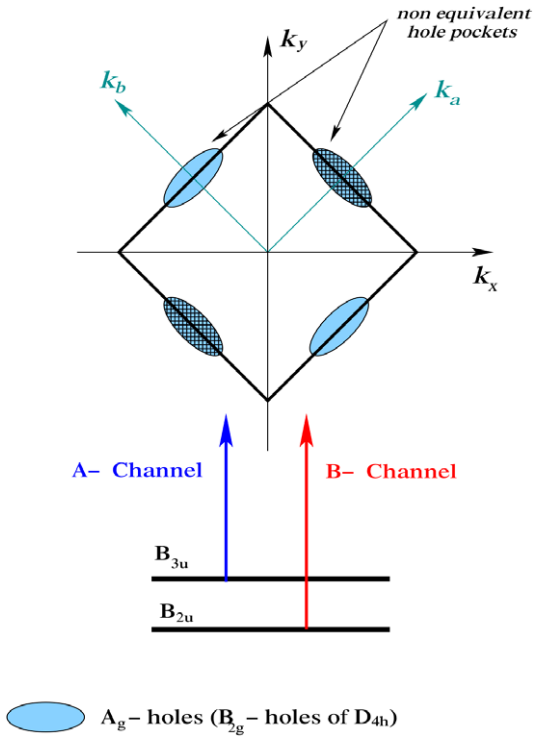

Figure 3. Photoionization of acceptor states in 3% doped $La_{2-x}Sr_xCuO_4$ for the allowed optical transitions according to the selection rules for the polarization of incident light. Only the two lowest-energy states are shown for clarity. The B_{2g} valence band holes of D_{4h}, located close to $(\pm\pi/2, \pm\pi/2)_g$ (in units $a = 1$), have their symmetry reduced to A_g of D_{2h}, and this determines the possible electric-dipole transitions for the $A(B)$-channel, where $E \parallel a(b)$, here in blue/left (red/right).

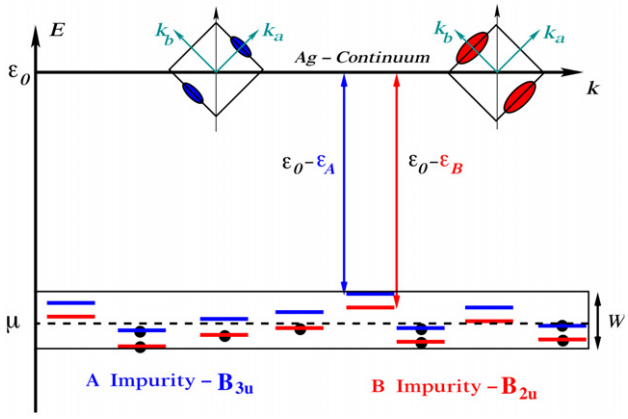

Figure 4. Localized deep and shallow acceptor states, as well as continuum states, for $x = 0.03$. The energy axis is reversed. A bandwidth W allows for empty sites above μ and sites with two holes below μ. Both B_{2u} and B_{3u} states are partially occupied at $T = 0$, in fractions of δ_A and δ_B, and provide different populations of pockets at $T \neq 0$.

acceptor sites above the chemical potential and, as imposed by charge neutrality, acceptor sites with two holes below it, see figure 4. Furthermore, since each p-wave state is associated with one spin projection, the bandwidth W should increase with increasing frustration, which distorts the AF background,

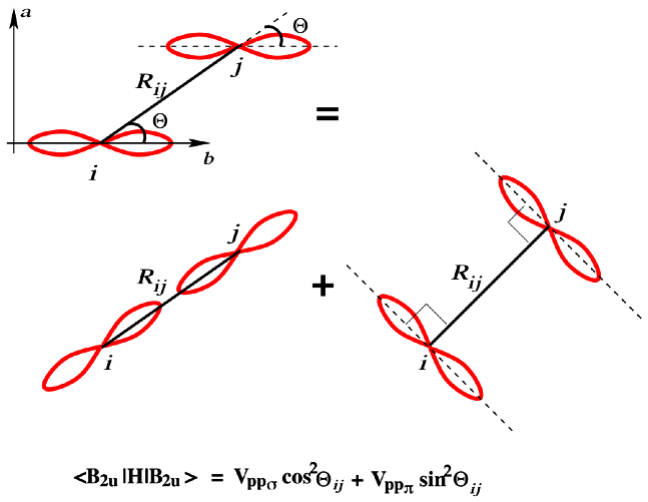

Figure 5. The overlap between two misaligned p-wave orbitals, where H represents the phonon absorption/emission Hamiltonian, that causes the jump of the holes from one site to another. $V_{pp\sigma}$ is the hybridization due to σ-overlaps (aligned orbitals) and $V_{pp\pi}$ is the hybridization due to π-overlaps (parallel orbitals). Usually $V_{pp\pi} \ll V_{pp\sigma}$, and we can neglect the second term.

mixing the two sublattices and broadening the peaks seen in the ac spectrum.

Observe that, even though double occupancy of the B_{2u} or B_{3u} orbitals individually is forbidden, due to the large on-site Coulomb repulsion U, configurations with one hole at each of the B_{2u} and B_{3u} levels at the same impurity site are allowed. Although the associated nearest-neighbor Coulomb interaction, V, may significantly correct the position, $\varepsilon_{A,B}$, and bandwidth, W, of the localized levels, it does not affect the splitting pattern between the levels nor mix their symmetries. This situation is analogous to the problem of placing two electrons at one p-orbital in the hydrogen atom. The energy is shifted but the pattern of Zeeman splitting is not modified.

Finally, the fraction of empty B_{2u} states above μ in figure 4, $1 - \delta_B$, is equal to filled B_{3u} states below it, δ_A, and the number of carriers participating in hopping conductivity for both channels is the same.

4. Dc conductivity

4.1. Phonon-assisted hopping between p-orbitals

According to the standard theory for hopping conductance in doped semiconductors, the conductance due to phonon-assisted hopping between two p-wave-like orbitals at sites i and j, separated by a distance $\mathbf{R}_{ij}$, is

$$G_{ij} = (G_0^{\sigma}\cos^2\Theta_{ij} + G_0^{\pi}\sin^2\Theta_{ij})^2 \left\{e^{-\Delta E_{ij}/k_B T} e^{-2R_{ij}/\xi}\right\}, \quad (14)$$

where ΔE_{ij} is the energy difference between the two impurity sites and Θ_{ij} is the angle between $\mathbf{R}_{ij}$ and the principal axis of the p-wave-like orbitals, see figure 5.

The dependence on the $\cos^2\Theta_{ij}$ and $\sin^2\Theta_{ij}$ terms in the above expression comes from the fact that the conductance is proportional to the square of the overlap integral between initial and final localized states, $G_{ij} \propto I_{ij}^2$. For B_{2u} states, for example, we have

$$I_{ij} = \langle B_{2u}(\mathbf{r}_i)|H_{ph}|B_{2u}(\mathbf{r}_j)\rangle = V_{pp\sigma}\cos^2\Theta_{ij} + V_{pp\pi}\sin^2\Theta_{ij}, \quad (15)$$

where $V_{pp\sigma}$ and $V_{pp\pi}$ are, respectively, the overlap integrals between direct, σ-type, and parallel, π-type, alignment between two p-orbitals, as can be seen in figure 5 and H_{ph} is the usual electron–acoustic–phonon Hamiltonian.

Note that usually $V_{pp\pi} \ll V_{pp\sigma}$, and we can safely neglect the second term in the above expression. A more quantitative estimate of the above integral would require the precise knowledge of the envelope wavefunction, also including the effects of correlations, in order to calculate the Coulomb (α) and resonant (β) integrals of the simplified LCAO (linear combination of atomic orbitals) theory, and this is beyond the scope of this paper.

Note, furthermore, that for fully symmetric, long wavelength acoustic A_g phonons (the case considered here) we have

$$\langle B_{2u}(\mathbf{r}_i)|H_{ph}|B_{3u}(\mathbf{r}_j)\rangle = \langle B_{3u}(\mathbf{r}_i)|H_{ph}|B_{2u}(\mathbf{r}_j)\rangle = 0, \quad (16)$$

by symmetry, and consequently no cross hopping between B_{2u} and B_{3u} states can occur. We anticipate that this very important property will play a crucial role in determining the dc anisotropies observed experimentally. Following the above reasoning, in what follows we will neglect the $V_{pp\pi}$ contribution to conductance and consider only the $V_{pp\sigma}$ contribution:

$$G_{ij} = G_0 \cos^4\Theta_{ij} \left\{e^{-\Delta E_{ij}/k_B T} e^{-2R_{ij}/\xi}\right\}, \quad (17)$$

where

$$G_0 = (G_0^{\sigma})^2. \quad (18)$$

The above result has a very important physical consequence. Hopping corresponding to parallel, π-type alignment between p-wave-like orbitals contributes a very high resistance to transport and becomes disconnected from the resistance network. The above statement simply reflects the fact that, when $\mathbf{R}_{ij}$ is perpendicular to the p-waves, $\Theta_{ij} = \pi/2$ and $G_{ij} = 0$.

We can give as an example a network of only B_{2u} states, represented by the red p-wave-like orbitals aligned horizontally, σ-type alignment, as shown in figure 6. For $E \parallel B_{2u}$, that is, for $E \parallel b$, it is clear that there are many low resistance links, along the direction of the largest overlap, and the phonon-assisted hopping involves mainly B_{2u} orbitals. For $E \perp B_{2u}$ or $E \parallel a$, however, π-type direct links between B_{2u} orbitals are disconnected (black dashed lines in figure 7) because they contribute a very high resistance to the problem. If we had only B_{2u} orbitals available, there could still be transport for $E \parallel a$, but in this case the way to make a hole hop vertically would be by using a nontrivial, zigzag path, as shown in figure 7, also resulting in a high resistance path. Fortunately, we also have available the B_{3u} orbitals, which, for $E \parallel a$, provide the direct, σ-type overlaps that produce a low resistance path, and thus they dominate the conductance at low temperatures, see figure 7.

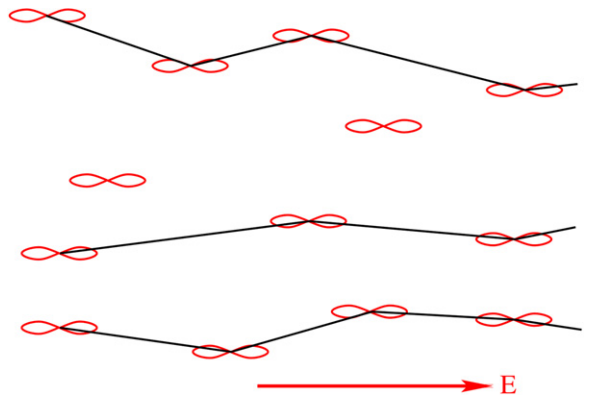

Figure 6. For $E \parallel b$ (here chosen to be the horizontal direction), there are many low resistance links between B_{2u} orbitals in red, σ-type overlap, giving rise to a large conductance and dominating the transport along this direction.

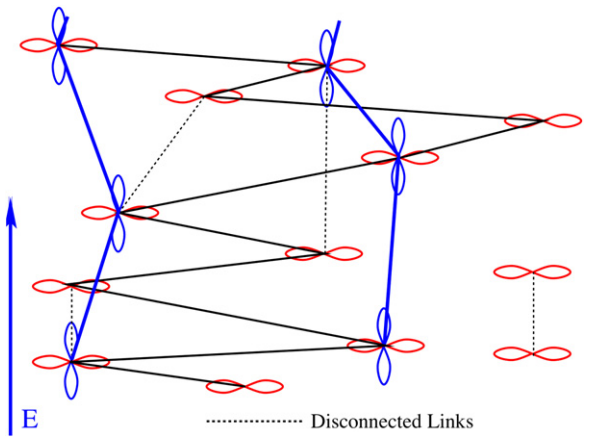

Figure 7. For $E \parallel a$ (here chosen to be the vertical direction), in turn, there are only high resistance links between B_{2u} orbitals in red, π-type overlaps (dotted black line) or zigzag hopping (thin black line), giving rise to negligible conductance. However, we also have available the higher energy B_{3u} states in blue, which are partially filled with holes even at $T = 0$ due to the finite bandwidth W. These B_{3u} states provide the necessary low resistance links for $E \parallel a$ through a direct σ-type overlap, and therefore dominate the conductance along this direction. The difference in the localization lengths for the two available orbitals for hopping conductance, $\xi_{B_{2u}} \neq \xi_{B_{3u}}$, renders the dc hopping transport anisotropic (see text).

4.2. Hopping conductance

When the temperature is still reasonably high the hole at site i can hop to its nearest impurity site j, as long as this is not already occupied. This is the so-called nearest impurity hopping (NIH) regime [23]. The conductivity is calculated by replacing in (14) $\langle R_{ij}\rangle = \tilde{R}$, $\langle \Delta E_{ij}\rangle = \epsilon_c$ and averaging out $\langle \cos^4 \Theta_{ij}\rangle$, where $\tilde{R}$ and ϵ_c are, respectively, the average inter-impurity distance and energy difference. The result is a simple activated behavior like

$$\sigma_{\mathrm{NIH}}(T) = \sigma_0 \exp\left[-\left(\frac{\epsilon_c}{k_B T}\right)\right]. \tag{19}$$

When the temperature is very small, however, G_{ij} is determined by the critical conductance G_c of a percolated

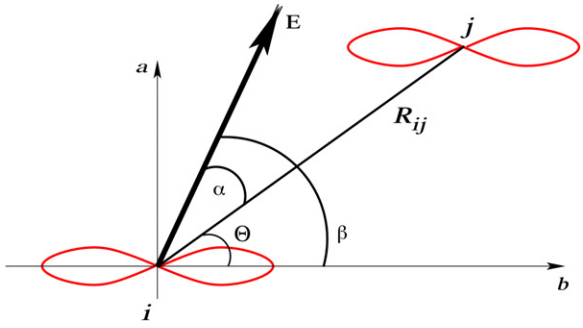

Figure 8. Geometry associated with the calculation of the anisotropic dc conductivity (see text).

random resistance network (RRN) [24]. In this case, the maximum: (i) carrier jump distance $R_{\max}$, (ii) energy difference $\Delta E_{\max}$, and (iii) angle $\Theta_{\max}$, are constrained through the density of states. The result is Mott's variable range hopping (VRH), that for $d = 2$ is [12]

$$\sigma_{\mathrm{VRH}}(T) = \sigma_0 \exp\left[-\left(\frac{T_0}{T}\right)^{1/3}\right], \tag{20}$$

where

$$T_0 = \frac{2\nu_c^{\max}}{k_B N_\Theta(\mu)\xi^2}, \tag{21}$$

and $\nu_c^{\max}$ is a geometrical constant depending on the solid angle determined by $2\Theta_{\max}$ (for the isotropic VRH case $2\Theta_{\max} = 2\pi$). Both ϵ_c and T_0 decrease with doping, and the crossover between NIH and VRH regimes occurs at

$$\epsilon_c = -\frac{\mathrm{d}\ln(\sigma_{\mathrm{VRH}}(T))}{\mathrm{d}\beta}, \tag{22}$$

with $\beta = 1/k_B T$ [23].

4.3. Dc hopping conductivity anisotropy

The dc conductivity for an arbitrary direction of the electric field receives a contribution from both channels, $\sigma_{B_{2u}}(T)$ and $\sigma_{B_{3u}}(T)$, where $\sigma_{(B_{2u},B_{3u})}(T)$ are hopping conductivities, either VRH or NIH, between two $B_{(2u,3u)} \rightarrow B_{(2u,3u)}$ states. We consider only hopping assisted by A_g phonons, in which case the cross-hopping $B_{2u} \rightleftharpoons B_{3u}$ vanishes by symmetry (even when assisted by B_{1g} phonons, such processes are exponentially suppressed at low temperature due to the further energy splitting between initial and final states).

Most importantly, the conductivity is proportional to the square of the carrier distance jump projection into the direction of the electric field, $(\mathbf{R}_{ij}\cdot\hat{\mathbf{e}})^2$, that is, proportional to $\cos^2(\alpha)$, as shown in figure 8. For this reason, the conductivity due to B_{2u} orbitals for an arbitrary direction of the applied electric field, $\hat{e}$, can be calculated through

$$\sigma_{B_{2u}}^{\hat{e}} = \sigma_{B_{2u}}^{\mathrm{VRH}}(T) \int_{-\Theta_{\max}}^{\Theta_{\max}} \cos^4\Theta \cos^2(\beta - \Theta)\,\mathrm{d}\Theta, \tag{23}$$

where β is the angle between $\hat{\mathbf{e}}$ and the B_{2u} orbital. An analogous expression can be found for the B_{3u} case, where

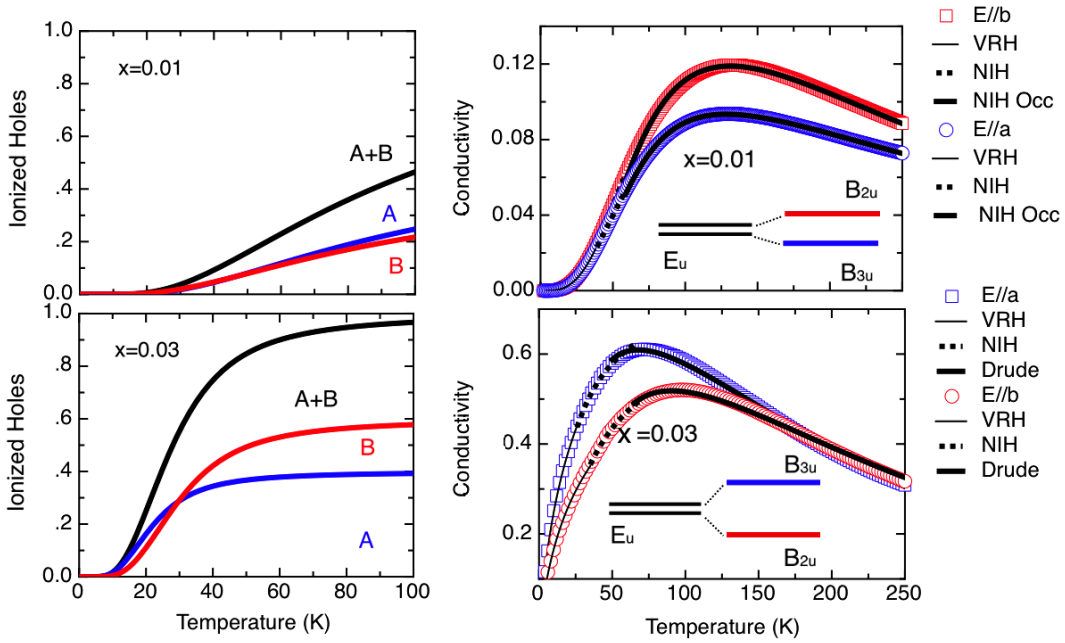

Figure 9. Left: fraction of thermally ionized holes. Right: dc conductivities, in $(\mathrm{m}\,\Omega\,\mathrm{cm})^{-1}$, for $x = 0.01$ and 0.03, for the variable range hopping (VRH), nearest impurity hopping (NIH) and weighed by the thermal occupation probability (NIH Occ) and Drude (Drude) regimes.

one has, instead, $\sin^2(\beta - \Theta)$ inside the integral, see figure 8. Now, for $E \parallel a, b$ and $\Theta_{\max} \ll \pi/4$, we have $\sigma^a_{B_{3u}}/\sigma^b_{B_{3u}} \gg 1$ for the B_{3u} channel and $\sigma^a_{B_{2u}}/\sigma^b_{B_{2u}} \ll 1$ for the B_{2u} channel, showing that the conductivity for $E \parallel a$ is dominated by $\sigma_A(T) \approx \sigma^a_{B_{3u}}(T)$, while for $E \parallel b$ it is dominated by $\sigma_B(T) \approx \sigma^b_{B_{2u}}(T)$. Finally, the orthorhombic splitting between these two channels, with $\xi_{B_{3u}} \neq \xi_{B_{2u}}$, renders the dc hopping conductivity anisotropic.

4.4. Drude regime

At high temperature the doped holes are ionized from the B_{3u} and B_{2u} impurity levels to occupy the valence band pocket states at $\mathbf{k}^{\pm}_a$ and $\mathbf{k}^{\pm}_b$, respectively, see figure 4. For $E \parallel a(b)$, the transport is predominantly due to the coherent holes with momenta along $\mathbf{k}_a(\mathbf{k}_b)$ and mass m^*, and a simple Drude model

$$\sigma^{A,B}_{\mathrm{Drude}} = \frac{\langle n^{A,B}_{2D}\rangle e^2\tau}{c_0 m^*}, \tag{24}$$

suffices to describe the experimental data. Here e is the electric charge, $c_0 = 6.6$ Å is the interlayer distance and $1/\tau$ is the relaxation rate. The activation of carriers is considered through the average thermal occupation [25]:

$$\langle n^{A,B}_{2D}\rangle = \frac{2\,n^0_{2D}\delta_{A,B}}{1+\sqrt{1+4g(n^0_{2D}/\mathcal{N}_0)\mathrm{e}^{\beta\varepsilon^{A,B}_f}}}, \tag{25}$$

where $g = 2$ accounts for pseudospin (sublattice) degeneracy, $\mathcal{N}_0 = N_0\,T$, with N_0 being the two-dimensional density of states, $\delta_{A,B}$ are the $T = 0$ fractions of $B_{3u,2u}$ impurities, satisfying $\delta_A + \delta_B = 1$, $\varepsilon^{A,B}_f = (\varepsilon_0 - \varepsilon_{A,B})$ are the freezing-out (or binding) energies and $n^0_{2D} = x/a^2$.

5. Comparison with experiments

In figure 9 we compare theory and dc conductivity data for $x = 0.01, 0.03$.

(i) For $4g(n^0_{2D}/\mathcal{N}_0)\mathrm{e}^{\beta\varepsilon^{A,B}_f} \gg 1$, low T, σ_{Drude} is exponentially suppressed and the data are well fitted using the σ_{VRH} and σ_{NIH} expressions (20) and (19), respectively.

(ii) For $4g(n^0_{2D}/\mathcal{N}_0)\mathrm{e}^{\beta\varepsilon^{A,B}_f} \ll 1$, instead, at higher T, when most of the holes are ionized, σ_{Drude} dominates and we can use equation (24).

(iii) Finally, we use $1/\tau(T)$ data obtained from fits to the mobility $\mu = e\tau/m^*$ [8], parameterized by the simple Fermi liquid expression $1/\tau(T) = 1/\tau_0 + \alpha T^2$.

5.1. $x = 0.01$

We find: (i) $T^A_0 = 32\,829$ K, $\epsilon^A_c = 125.09$ K and $\delta_A = 0.52$, for $E \parallel a$, and (ii) $T^B_0 = 30\,878$ K, $\epsilon^B_c = 99.97$ K and $\delta_B = 0.48$, for $E \parallel b$. The ratio $T^A_0/T^B_0 = \varepsilon^A_f/\varepsilon^B_f > 1$, indicating that the B_{3u} state is the ground state, is slightly more populated and the splitting is small. We used $\varepsilon^A_f = 200$ K, $\varepsilon^B_f \approx 180$ K and $N_0 \approx 1.8 \times 10^{-3}\ \mathrm{K}^{-1}/a^2$. We note that the NIH regime extends up to 250 K, weighed by thermal occupation.

5.2. $x = 0.03$

We find: (i) $T^A_0 = 94.38$ K, $\epsilon^A_c = 15.2$ K and $\delta_A = 0.4$, for $E \parallel a$, and (ii) $T^B_0 = 107.2$ K, $\epsilon^B_c = 24.1$ K and $\delta_B = 0.6$, for $E \parallel b$. Notice that we now have $T^A_0/T^B_0 = \varepsilon^A_f/\varepsilon^B_f < 1$ and the B_{2u} state becomes the ground state. The B_{2u} and B_{3u} splitting is much larger, around 30 K, in agreement with [7]. We used $\varepsilon^B_f = 110$ K and $\varepsilon^A_f \approx 80$ K [7], and we use the same value for N_0.

5.3. Anisotropy switch at high T

Due to the existence of two regimes for conductivity, hopping and Drude, a switch of anisotropies is expected to occur at high T [11]. For $x = 0.02$–0.04, we find $\sigma_A > \sigma_B$ at very low T, since they all have a B_{2u} ground state, while $\sigma_A < \sigma_B$ at high T [11], since $\langle n^A_{2D}\rangle < \langle n^B_{2D}\rangle$, see figure 9. For $x = 0.01$, which has a B_{3u} ground state, the same analysis applies. However, since $\langle n^A_{2D}\rangle$ is only slightly larger than $\langle n^B_{2D}\rangle$, we observe a smooth convergence of conductivities for 120 K $< T <$ 250 K, figure 9, and a regime with $\sigma_A > \sigma_B$ would occur only at much higher T (not measured).

The values for $n^0_{3D} = n^0_{2D}/c_0$, $m^* \approx 4m_e$ and $\varepsilon^{A,B}_f$ are all consistent with the Hall coefficient [26] and optical conductivity [7, 27].

6. Conclusions

In lightly doped $La_{2-x}Sr_xCuO_4$, strong correlations open a Mott gap in the spectrum and antiferromagnetic interactions place the top of the valence band close to the pockets centered at $(\pm\pi/2, \pm\pi/2)$. These very same AF interactions stabilize a parity-odd ground state for a hole bound to the Sr impurity when the Coulomb trap potential is taken into account. Then, the peculiar ac and dc responses can be promptly described using basic concepts from p-type semiconductor physics, and well grounded concepts from group theory and selection rules. In particular, all the novel anisotropies arise from the parity-odd, rotational-symmetry-broken deep and shallow acceptor levels, which are split by orthorhombicity in the case of $La_{2-x}Sr_xCuO_4$.

Acknowledgments

MBSN acknowledges fruitful discussions with J Falb, R B Capaz, R Gooding, B Koiller, V Kotov, A Muramatsu, and O Sushkov. YA is supported by KAKENHI 19674002 and 20030004.

References

[1] Lee P A, Nagaosa N and Wen X G 2006 *Rev. Mod. Phys.* **78** 17
[2] Chang J *et al* 2008 *New J. Phys.* **10** 103016
[3] Doiron-Leyraud N *et al* 2007 *Nature* **447** 565
[4] Jaudet C *et al* 2008 *Phys. Rev. Lett.* **100** 187005
[5] Comanac A *et al* 2008 *Nature Phys.* **4** 287–90
[6] Lavrov A *et al* 2001 *Phys. Rev. Lett.* **87** 017007
Gozar A *et al* 2004 *Phys. Rev. Lett.* **93** 027001
Ando Yoichi *et al* 2004 *Phys. Rev. Lett.* **93** 267001
[7] Dumm M *et al* 2003 *Phys. Rev. Lett.* **91** 077004
Padilla W J *et al* 2005 *Phys. Rev.* B **72** 205101
[8] Yoichi A *et al* 2001 *Phys. Rev. Lett.* **87** 017001
[9] Vollhardt D and Wölfle P 1980 *Phys. Rev. Lett.* **45** 842
Vollhardt D and Wölfle P 1980 *Phys. Rev.* B **22** 4666
[10] Basov D N, Dabrowski B and Timusk T 1998 *Phys. Rev. Lett.* **81** 2132
[11] Yoichi A *et al* 2002 *Phys. Rev. Lett.* **88** 137005
[12] Shklovskii B I and Efros A L 1984 *Electronic Properties of Doped Semiconductors* (Berlin: Springer)
[13] Benfatto L and Morais Smith C 2003 *Phys. Rev.* B **68** 184513
Lorenzana J and Seibold G 2003 *Phys. Rev. Lett.* **90** 066404
Homes C C *et al* 2003 *Phys. Rev.* B **67** 184516
[14] Kotov V and Sushkov O P 2005 *Phys. Rev.* B **72** 184519
[15] Chen Y, Rice T M and Zhang F C 2006 *Phys. Rev. Lett.* **97** 237004
[16] Rabe K M and Bhatt R N 1991 *J. Appl. Phys.* **69** 4508
[17] Gooding R J 1991 *Phys. Rev. Lett.* **66** 2266
[18] Kohn W and Luttinger J M 1955 *Phys. Rev.* **98** 915
[19] Silva Neto M B in preparation
[20] Sushkov O P *et al* 2008 *Phys. Rev.* B **77** 035124
[21] Gozar A, Seiki K, Yoichi A and Blumberg G 2005 *Frontiers in Magnetic Materials* ed A V Narlikar (Berlin: Springer) pp 755–89
[22] Tassini L *et al* 2005 *Phys. Rev. Lett.* **95** 117002
[23] Lai E and Gooding R J 1998 *Phys. Rev.* B **57** 1498
[24] Ambegaokar V, Halperin B I and Langer J S 1971 *Phys. Rev.* B **4** 2612
[25] Ibach H and Lüth H 2002 *Solid State Physics* (Berlin: Springer)
[26] Yoichi A *et al* 2004 *Phys. Rev. Lett.* **92** 197001
[27] Padilla W J *et al* 2005 *Phys. Rev.* B **72** 060511